# An experimental study of the correlation between surface roughness and light scattering for rough metallic surfaces

Hongsong Li and Kenneth E. Torrance
Program of Computer Graphics, Rhodes Hall, Cornell University, Ithaca, NY 14853

## ABSTRACT

We present an experimental study of the angular distribution of light scattered from several rough metallic surfaces, which cover a range of roughness conditions. The substrate materials are steel or glass; roughened by bead-blasting, grinding, or etching; and aluminum-coated. The measured surface-roughness statistics are filtered by using a composite roughness model. The raw mechanical roughnesses range from $0.21\mu$m to $2.66\mu$m; the high-frequency small-scale roughnesses range from $0.13\mu$m to $0.86\mu$m. The optical wavelength is 550nm, so that the roughness-to-wavelength ratio is of order one. A BRDF model based on the Kirchhoff approximation is used to establish a relationship between surface-height statistics and the angular distribution of the scattered light. Angular distributions calculated with the BRDF model are fit to the measurements. The best-fit roughness statistics from the BRDF model agree closely with those measured for the high-frequency small-scale roughness component. The latter roughness component, which has the highest surface slopes, is thus the primary contributor to the angular distribution of the reflected light. We show that the Kirchhoff approximation can be applied to rough metallic surfaces that have multiple scales of roughness and near-, but not perfect, Gaussian surface-height distributions.

**Keywords:** Optics, scattering, roughness, surfaces, reflectance, BRDF, Kirchhoff approximation, computer graphics

## 1. INTRODUCTION

Efficient analytical models for the light scattered by a surface are needed in computer graphics in order to create photorealistic images of synthetic scenes and environments.[1] The directional light scattering by a rough surface represents one example. Physically-based (wave-optics) models have been developed for this purpose, but the models need to be verified by experiments. To use such a model, we also need a practical method to estimate the surface-roughness statistics, either by direct measurement or inferred approximation. In this paper, we examine the usefulness of an existing wave-optics reflectance model,[2] which is based on the Kirchhoff approximation,[3,4] for roughened metallic surfaces and propose a method of surface-height characterization.

### 1.1. Analytical models for the BRDF

The directional properties of light reflection at a surface can be characterized over the entire angular and wavelength domains by the bidirectional reflectance distribution function (BRDF).[5]

For use in computer graphics, a BRDF model should be efficient, accurate, and easy to use. Millions of BRDF evaluations are required to get quality images even for a simple synthetic scene. Compact analytical models are preferred. Further, the BRDF model should cover the entire incident and reflection hemispheres, and the visible wavelength range, with good accuracy. This allows the rendering of surfaces under arbitrary orientations and lighting, with correct color reproduction. Lastly, the inputs for use of a BRDF model should be intuitive and easy to determine.

Limited by computational power, the early BRDF models in computer graphics emphasized efficiency more than accuracy, following an empirical apporach.[6–8] To improve the models, advancements from optics were introduced.[2,9,10] Among these, BRDF models employing the Kirchhoff approximation were promising due to their relative simplicity, analytical form, ease of computation, accuracy, and statistical representation of rough surfaces. The scalar form of the Kirchhoff approximation was developed by P. Beckmann[3] and a more general vector form by A. Stogryn.[4] The latter allows for a full Fresnel reflectivity and polarization. Based on the foregoing, X. He et al.[2] proposed a comprehensive BRDF model (He-Torrance model hereafter) for computer graphics applications. The model incorporates the vector form,[4] the masking/shadowing factor developed by B. G. Smith,[11] and applies for first-surface reflections. Any multiple scattering on the surface, or any possible subsurface scattering, were modeled with a constant Lambertian term. (More

Advanced Characterization Techniques for Optics, Semiconductors, and Nanotechnologies II, edited by Angela Duparré, Bhanwar Singh, Zu-Han Gu, Proceedings of SPIE Vol. 5878 (SPIE, Bellingham, WA, 2005)
0277-786X/05/$15 · doi: 10.1117/12.617637

details on the He-Torrance model and the basic equations are available in Appendix A.) Since the He-Torrance model is based on the Kirchhoff approximation, the validity of that approximation will directly affect any predictions.

The limitations and accuracy of the Kirchhoff approximation have been studied theoretically and experimentally. Generally, the Kirchhoff approximation is accurate when the radius of surface curvature (due to roughness elements, for example) is large compared with the illuminating wavelength and the angle of incidence is not large.[12] In addition, the accuracy may be limited by other assumptions of the theoretical model, such as a Gaussian distribution of surface heights, a single length scale of roughness, or a constant reflection coefficient.

### 1.2. Experimental validation of BRDF models

For computer graphics applications, experimental tests of BRDF models are somewhat limited. Several BRDF instruments were built and used to validate models.[10, 13–15] Perhaps the earliest BRDF measurements used by the computer graphics community were published by K. E. Torrance and E. M. Sparrow.[16] Those measurements were adopted to develop what is now known in the field as the Cook-Torrance model[9] and the He-Torrance model.[2] Unfortunately, none of the measurements provided ample angular and spectral coverage. For validating the He-Torrance model, the experimental studies included only limited measurements of the surface-heights of the samples.

In the optics community, extensive experimental investigations of light scattering have been carried out to validate various BRDF models. One classic study is that of K. A. O'Donnell and E. R. Mendez,[17] who took great efforts to fabricate perfectly Gaussian-distributed surfaces with a single scale of roughness. The surfaces were fabricated by lithography, which makes it possible to control the height statistics.[18] To validate the Kirchhoff approximation, the surface-heights of the surfaces were measured and analyzed. Next, the BRDFs of the surfaces were measured. Calculated directional reflectances based on the surface statistics agreed well with the measured reflectances. This success inspired more experimental work to study surfaces fabricated with similar techniques.[19–22] Although these "perfect" samples led to good agreement between the theory and the experimental results, the applicability of the Kirchhoff approximation for real-world surfaces was still not verified, since such surfaces may not have near-Gaussian surface-height distributions or may have multiple scales of roughness.

Experimental studies of light scattering and surface-height statistics were also carried out for "less perfect" samples, such as aluminized ground glass,[23] magnesium oxide ceramic,[16] fused polycrystalline aluminum oxide,[24] hand-lapped stainless steel,[25] diamond-turned brass/nickel,[26] and epoxy coatings.[27] The agreement between theory and measurement was less satisfactory, compared with "perfect" surfaces. E. Marx and T. V. Vorburger[25] studied the relation between the surface-heights of hand-lapped stainless steel (measured with a stylus profilometer) and the angular distribution of light scattering (measured with a laser scatterometer). A theoretical model, based on the scalar form of the Kirchhoff approximation, was used to compute the scattering intensity with the height statistics; on the other hand, the model was also fit to the measurements to obtain the height statistics. Multiple scales of roughness were rarely considered, a fact that may partially explain the discrepancies between measured and calculated results.

One approach to describe the light scattering from rough surfaces with multiple roughness scales is to use composite roughness models.[28–30] Such models divide a rough surface into two independent components: a high-frequency small-scale roughness riding on a low-frequency large-scale roughness. The light scattered by these two components is treated separately by using either a perturbation or a Kirchhoff approach, depending on the height statistics. However, it is impractical to directly use the composite models for computer graphics because of their complexity. Another approach is to measure the surface-heights and to isolate the roughness scale (or the spatial bandwidth) that dominates scattering behavior. E. Marx and T. V. Vorburger[25] realized the importance of the spatial bandwidth selection. They filtered their surface-height data to attenuate spatial wavelengths $> 50\mu$m. The roughness statistics of the filtered data agreed better with that inferred by fitting a BRDF model to the optical measurements. However, this filtering technique did not have a theoretical basis.

The first purpose of the present paper is to provide measured data on light scattering with sufficient angular and spectral coverage for computer graphics applications. Second, we want to examine the usefulness of the He-Torrance model for some real-world metallic surfaces. Third, a practical method is proposed to characterize such surfaces and to generate input roughness parameters for the He-Torrance model. The revised surface-height statistics can help to predict the angular distribution of scattered light for visual appearance simulations. For simplicity, we limit our effort to metallic surfaces and the visible light spectrum.

## 2. SURFACE PREPARATION AND CHARACTERIZATION

Five isotropic metallic surfaces were fabricated with three preparation methods. Surface-height measurements and a composite roughness model are presented. Table 1 provides a list of the samples and some measured and inferred roughness statistics.

### 2.1. Preparation of rough surfaces

We chose two substrate materials (steel and glass plates) and three methods of surface preparation: bead-blasting, grinding, and etching. Our objective was to prepare uniform (less than $\pm 10\%$ non-uniformity), large (larger than 100mm $\times$ 100mm), and isotropic surfaces.

With bead-blasting, very small, perfectly round beads are propelled by high pressure air to remove/deform the top layer of a surface. This is a numerous, random, and cumulative process resulting in a Gaussian surface. An industrial bead-blaster was used (with glass beads of 0.25mm diameter). The air pressure was adjusted to fabricate surfaces with different roughness heights. Surfaces BBQAL1 and BBQAL2 were processed with air at 690kPa and 138kPa, respectively. The substrates of these test surfaces are Q-panels (R-46), a reference steel panel (100mm $\times$ 125mm) used for the paint and manufacturing industries. More than 10 minutes of blasting guaranteed the randomness of the process.

Abrasive grinding usually results in non-Gaussian surfaces. Since the surface-heights generated by this process are determined by the largest grinding grit, this process is random but not cumulative. We used a Buehler Nelson-Zimmer®2000 system to grind two pieces of 125mm $\times$ 125mm window glass. Grinding powders with two grit sizes, 120grit and 240grit, were used to fabricate test samples GGAL120 and GGAL240, respectively. More than five hours of grinding guaranteed the randomness and uniformity. A microscope was used to inspect the finished surfaces; the ground glass surfaces look "jagged."

The last method is etching, which may or may not result in a Gaussian surface. The uncertainty arises because the etching process is influenced by the material's microstructure. Therefore, etching is not completely random. The test sample, NGGAL, is commercial, acid-etched, non-glare glass (125mm $\times$ 125mm).

A thin film of pure aluminum was deposited on each test surface with a CHA RAP-600 Thermal Evaporator. The film has a thickness of approximately 50nm, so that no light energy transmitted through the film. Thus, subsurface light scattering can be neglected.

### 2.2. Characterization of rough surfaces

A surface measurement instrument, a Tencor Alpha Step 500 Surface Profiler, was used to measure the surface-heights (or profiles) of the test samples. This is a stylus-traversing instrument that provides $z(x)$ height data with 1-Angstrom (1Å) vertical and $0.1\mu$m horizontal resolutions. For each test surface, nine measurements were taken in randomly chosen regions and in random directions. Each height measurement consists of 4000 data points, which represents a $400\mu$m traverse.

The height data were analyzed statistically. For a random rough surface, the vertical and horizontal height distributions can be respectively described by the height probability distribution function (PDF) and the spatial autocorrelation function (ACF). Though not normalized, the histogram of the height data can be used as the PDF. The ACF $\rho(\beta)$ is given by:

$$\rho(\beta) = \lim_{L\to\infty} \frac{\int_0^L z(x)z(x+\beta)dx}{\int_0^L z(x)^2 dx} \tag{1}$$

where $L$ is the stylus traverse length. When both the PDF and the ACF conform to a Gaussian (normal) distribution, the surface is said to be Gaussian. The PDF and ACF are qualitative descriptions; we need both to evaluate a departure from Gaussian behavior. Quantitative measures of the PDF and ACF are respectively provided by the root mean square (RMS) roughness height $\sigma$ and the horizontal autocorrelation length $\tau$. Both are e-folding lengths associated with exponentials. The RMS roughness $\sigma$ can also be obtained from:

$$\sigma = \sqrt{\frac{1}{L}\int_0^L z(x)^2 dx} \tag{2}$$

The slope of a rough surface is here taken as the ratio of the RMS roughness to the autocorrelation length, namely, $\sigma/\tau$. These quantities are used as inputs for the He-Torrance and many other BRDF models.

## 2.3. Separation of roughness length scales

Care is required in interpreting the foregoing statistical measures, as real-world surfaces may have a wide range of roughness length scales. Among them, only a limited range (of spatial bandwidths) are relevant for computer graphics applications; in particular, only those dominating the directional scattering of visible light.

Using computational studies of the light scattered from surfaces with multiple roughness length scales, Y. Yang and R. O. Buckius[31] determined that the roughness domain with the largest slope dominated the directional scattering distributions. This provides the basis for our roughness model. We assume that our measured surface-heights can be divided into two roughness components: a high-frequency small-scale component and a low-frequency large-scale component. For our data, the high-frequency small-scale component turned out to have the highest slopes. We thus used a high-pass filter on our measured roughness data for each surface to filter out the large-scale components. The lengths of the large-scale components that were filtered out were about 25$\sim$40$\mu$m, varying from surface to surface. The shortest filter, $25\mu$m, is about 50 times the incident wavelength. Our filter length scales are close to the filter length used by E. Marx and T. V. Vorburger $(50\mu\text{m})$.[25]

The foregoing is illustrated graphically in Figure 1. The results of one measurement of $z(x)$ for the roughest ground-glass surface, GGAL120, was divided into two components by filtering. Since the high-frequency small-scale component is expected to dominate the scattered light directional distributions, we focus on the statistics of that component. The low-frequency large-scale component will be neglected. Although this simplified approach will bring errors to the statistical results, we believe that the error is acceptable for our applications.

For each test sample we did similar separations. We calculated the RMS roughness $\sigma$ and the autocorrelation length $\tau$ for the nine surface-height traverses, for both the raw height data and the high-frequency small-scale component (full results are available in a report[32]). We calculated the average and the standard deviation of $\sigma$ to assess spatial uniformity. Results for $\sigma$, $\tau$ and the slope $\sigma/\tau$ appear in Table 1. For convenience later, we append subscripts to these symbols: $r$ for the raw height data $(\sigma_r, \tau_r, (\sigma/\tau)_r)$, and $m$ (for measured) for the small-scale roughness data $(\sigma_m, \tau_m, (\sigma/\tau)_m)$. We selected the height measurements nearest the center of the surface to obtain the PDF and ACF graphs that are displayed later.

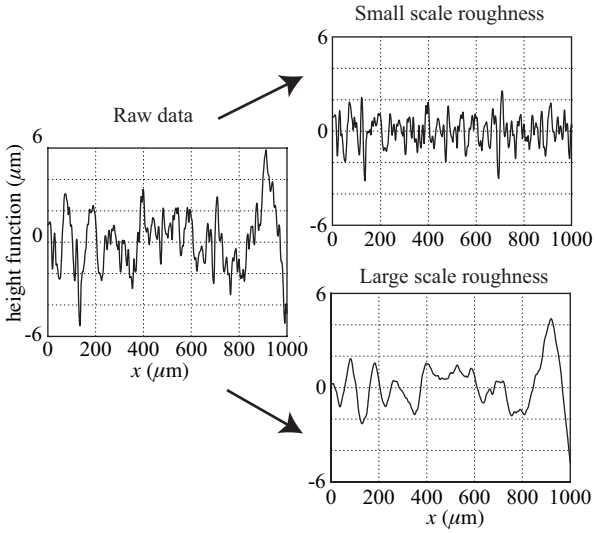


**Figure 1.** Separation of a mechanically-measured surface-roughness height scan into high-frequency (small-scale) and low-frequency (large-scale) components for the aluminized ground glass surface GGAL120.

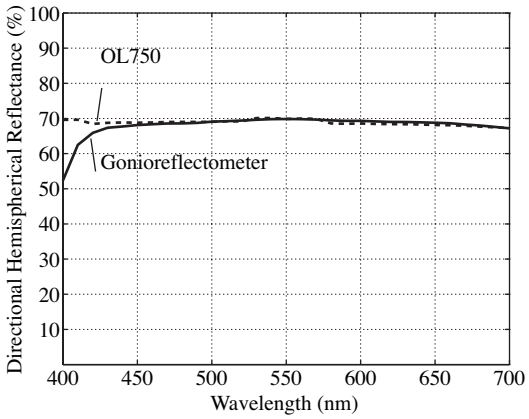


**Figure 2.** Comparison of directly-measured (OL750) and BRDF-integrated (gonioreflectometer) directional-hemispherical reflectances for aluminized bead-blasted steel surface BBQAL2 (smoothest steel, slope $(\sigma/\tau)_m = 0.084$), $\theta_i = 10^\circ$.

## 3. REFLECTANCE MEASUREMENTS

We measured BRDFs with a gonioreflectometer and directional-hemispherical reflectances with an Optronics OL-750 diffuse reflectometer. To illustrate measured results, we will use Figures 2 (on previous page), 5 and 6 (appearing later) which correspond to the smoothest bead-blasted steel substrate BBQAL2.

### 3.1. Measuring BRDF

The BRDF is the ratio of the radiance reflected from a surface in the direction $(\theta_r, \phi_r)$ to the irradiance onto the surface from the direction $(\theta_i, \phi_i)$.

$$f_r(\theta_i, \phi_i; \theta_r, \phi_r) = \frac{dL_r(\theta_i, \phi_i; \theta_r, \phi_r)}{dE_i(\theta_i, \phi_i)} \tag{3}$$

where $\theta_i$ and $\phi_i$ are the zenith and azimuthal angles of the irradiance, and $\theta_r$ and $\phi_r$ are the zenith and azimuthal angles of the reflected radiance. (The coordinate system is shown in Appendix A.) For an isotropic surface, only three angles are needed. The reflected radiance $dL_r$ and irradiance $dE_i$ have units of W/m$^2$sr and W/m$^2$, respectively.

An automated, three-axis BRDF measurement instrument, called a gonioreflectometer, was built in the Optical Measurement Laboratory at the Cornell Program of Computer Graphics.[33–35] The gonioreflectometer performs rapid measurements of the BRDF of flat, isotropic sample surfaces over the visible spectrum and over most of the incident and reflection hemispheres. Special design was applied to enable BRDF measurements at grazing angles up to and slightly above $85^\circ$. The spectroradiometric detector takes 31 convolved wavelength samples covering the visible spectrum (400nm–700nm) in one snapshot. For the measurements on our rough metallic surfaces, the BRDF values were obtained by a relative method, which compared the reflected signal from our test surfaces with that from a reference surface (Spectralon) with a known BRDF.

The flexible sampling mechanism of the gonioreflectometer enables us to sample the BRDFs in the plane of incidence, as well over the entire reflection hemisphere. Figure 5 shows BRDF measurements (the data points) in the plane of incidence for various illumination angles $\theta_i$. We also measured the BRDFs at uniformly-distributed sampling positions over the reflection hemisphere. For an incident direction of $10^\circ$ and a wavelength of 550nm, the BRDF in the reflection hemisphere is shown in Figure 6 (upper row). The vertical axis is the BRDF; the left and right orthogonal axes map the spherical coordinates above a surface. The plane of incidence goes through the peaks of the curves. The points are plotted in a uniform parameterization of the hemisphere such that each grid element in the plot represents a region of the hemisphere with the same solid angle.[36]

### 3.2. Measuring directional-hemispherical reflectance

The directional-hemispherical reflectance $\rho_{dh}$ is the ratio of the radiant power $dE_r$ reflected to the hemisphere to the radiant power $dE_i$ incident onto a surface, both in W/m$^2$.

The OL-750 system directly measures $\rho_{dh}$ for flat surfaces at an incidence angle of $10^\circ$ with a rated error of less than 1%. On the other hand, the BRDFs measured by the gonioreflectometer at an incident direction of $10^\circ$ were numerically integrated over the reflection hemisphere to obtain $\rho_{dh}$. Figure 2 shows a comparison of the integrated and directly-measured $\rho_{dh}$ for the smoothest steel surface BBQAL2. (Note: both instruments used Spectralon as their common reference surface.) In Figure 2, over the entire visible spectrum, the directional-hemispherical reflectance obtained from the integrated BRDF measurements is within 2% of the comparison values obtained by direct measurement. The only exception is at short wavelengths, below 420nm. The comparison suggests that the BRDF measurements are accurate in both magnitude and spectrum, with less than 2% integrated error.

For all the test surfaces, we measured the BRDFs in the plane of incidence and over the reflection hemisphere.[32] Limited by space, only representative results are shown later. With the OL-750 measurement data, we confirmed that the integrated accuracy of the BRDF measurements is generally within 2%. For computer graphics applications, the measurements provide sufficient accuracy as well as ample angular and spectral coverage.

**Table 1.** Measured and best-fit height statistics

| Sample | Description | Raw height data | | | Small-scale roughness data | | | | Best fit results | |
|---|---|---|---|---|---|---|---|---|---|---|
| | | $\sigma_r$ ($\mu$m) | $\tau_r$ ($\mu$m) | $(\sigma/\tau)_r$ | $\sigma_m$ ($\mu$m) | $\tau_m$ ($\mu$m) | $(\sigma/\tau)_m$ | Surface non-uniformity (+/-) | $(\sigma/\tau)_b$ | Uniform diffuse term $a_b$ |
| BBQAL1 | Aluminized Bead-blasted Steel | 2.58 | 27.2 | 0.095 | 0.72 | 5.6 | 0.129 | 3.9% | 0.119 | 0.70 |
| BBQAL2 | Aluminized Bead-blasted Steel | 1.24 | 30.5 | 0.041 | 0.54 | 6.5 | 0.084 | 6.8% | 0.080 | 0.37 |
| GGAL120 | Aluminized Ground Glass, 120grit | 2.66 | 41.6 | 0.064 | 0.86 | 5.6 | 0.154 | 4.5% | 0.166 | 0.44 |
| GGAL240 | Aluminized Ground Glass, 240grit | 1.63 | 24.0 | 0.068 | 0.61 | 4.7 | 0.130 | 4.1% | 0.158 | 0.44 |
| NGGAL | Aluminized Acid-etched Glass | 0.21 | 11.7 | 0.018 | 0.13 | 5.4 | 0.024 | 5.3% | 0.023 | 0.00 |

## 4. RELATING SURFACE-HEIGHT STATISTICS TO THE ANGULAR DISTRIBUTION OF SCATTERED LIGHT

The relation between surface-height statistics and the angular distribution of light reflected from a surface leads to inverse and direct scattering problems. The inverse problem is to fit a model (in this case, the He-Torrance model) to the BRDF measurements to obtain the surface-height statistics; the direct problem is to predict the BRDF of a surface from a measured set of surface-height statistics by using a BRDF model (here, also the He-Torrance model).

We start with the inverse problem. For a metallic surface, the He-Torrance model[2] contains five parameters: wavelength $\lambda$, RMS roughness $\sigma$, autocorrelation length $\tau$, index of refraction $n(\lambda)$, and a uniform-diffuse term $a(\lambda)$ (which allows for multiple surface scattering and/or subsurface scattering). Two of these parameters will either be independently specified $(\lambda)$ or found from tables $(n(\lambda))$.[37] For the roughness range of our metallic surfaces, the BRDF is determined predominantly by the roughness slope parameter $\sigma/\tau$. Thus, we need to find only the values of the slope $(\sigma/\tau)$ and the uniform-diffuse $(a(\lambda))$ parameters to achieve a fit. When a best fit has been found, we append the subscript $b$ to these parameters: $(\sigma/\tau)_b, a_b$ (see Table 1).

We used the nonlinear optimization function in Matlab which varies model parameters to minimize the fitting error between model and measured data. We used an energy-weighted root mean square fitting error:

$$\epsilon_{\textit{fitting}} = \sqrt{\frac{1}{N}\sum\left\{\left[f_{r,\textit{model}}(\theta_i;\theta_r,\phi_r) - f_{r,\textit{measured}}(\theta_i;\theta_r,\phi_r)\right]\times\cos\theta_r\right\}^2} \tag{4}$$

The functions $f_r$ (model and measured) depend on four independent variables $(\lambda;\theta_i;\theta_r,\phi_r)$ which span the measurement space. For simplicity, we elected to fit only at the midpoint of the visible spectrum $(\lambda = 550\text{nm})$. The cosine term in Equation 4 gives smaller weights to BRDF values at large grazing angles of reflection, where the absolute BRDF values can be several orders of magnitude larger than those in other parts of the reflection hemisphere. Otherwise, the large-magnitude differences in the BRDF values can bias a fitting. The fitting method appears to be robust and was independent of the initial values.

The direct problem is solved by employing the surface height statistics, specifically $(\sigma/\tau)_m$ found by mechanical measurement in Section 2, as an input to the BRDF model; also required as an input is the uniform-diffuse parameter $a(\lambda)$, for which we use the asymptotic values found (at $-\theta_r$) in the incidence-plane BRDF measurements (those values are within 10% of the $a_b$ reported in Table 1). Of course, there are intrinsic errors in the statistics measurements and also

variations over the surface due to surface non-uniformities. We allow for this and later provide upper and lower bounds for directly-calculated BRDFs from the He-Torrance model.

It is generally complicated to do rigorous data fitting for a nonlinear function like the BRDF. However, for our applications in computer graphics we may be able to relax some of those concerns, due to limitations in human vision, cameras, and display devices, such as polarization insensitivity and limited dynamic range. As a result, some effects like narrow retro-reflections and de-polarization can often be neglected; and the relative errors in BRDF predictions at very low or very high absolute magnitudes may not be perceptible to the eye. However, human vision is sensitive to surface glossiness, which affects the lateral shape and angular positions of the reflectance lobe, so these features should be accurately predicted by a reflectance model.

## 5. EXPERIMENTAL RESULTS

Results for the aluminized bead-blasted steel panels, the aluminized ground glass, and the aluminized acid-etched glass are given in the following sections. Since the reflecting metal, aluminum, has an almost flat reflectance spectrum over the visible region, we present results only for a single wavelength, $\lambda = 550$nm.

### 5.1. Bead-blasted steel panels with aluminum coating

For the two bead-blasted steel surfaces, BBQAL1 (roughest) and BBQAL2 (smoothest), the normalized height histograms and the autocorrelation functions (ACF) for the high-frequency small-scale component of the roughness are shown in Figure 3. The solid lines are the fits of Gaussian curves. For the histograms, the curves agree moderately well with the data, suggesting that the high-frequency small-scale component of the roughness is nearly Gaussian. For the autocorrelation functions ACF, the fitted curves agree very well with the data. Considering the random characteristics of the bead-blasting process, these results are expected.

Reflectance measurements for the two bead-blasted steel surfaces, BBQAL1 and BBQAL2, are presented in Figures 4 to 8; of these, Figures 4, 5, 7, and 8 are incidence-plane BRDFs, whereas Figure 6 displays BRDFs in the hemisphere. In the incidence-plane figures, the curves are results from the model. In Figures 4 and 5, the curves are the best-fit curves yielding *best fit slopes* $(\sigma/\tau)_b$; in Figures 7 and 8, the same measured data are shown, but the curves are calculated using the *measured slopes* $(\sigma/\tau)_m$ for the small-scale roughness. The upper/lower bounds were found by respectively varying the input slopes $(\sigma/\tau)_m$ by the -/+ amounts corresponding to the measured percentage non-uniformity in the roughness of the surface (see Table 1).

Results for the roughest and smoothest bead-blasted metal surfaces are shown, respectively, in Figures 4 and 5. The roughness to wavelength ratios are of order one, so a wave optics model is appropriate. Note the good agreement between measurements and the model. A similar comparison over the reflection hemisphere is shown in Figure 6 for the smoother surface.

For small angles of incidence ($10^\circ$ and $30^\circ$), the measurements shown in Figures 4 and 5 are Gaussian-like curves with maxima near or just beyond the specular angle. For $60^\circ$ incidence, off-specular maxima are apparent. Best-fit slope values for Figures 4 and 5 are $(\sigma/\tau)_b = 0.119$ and $0.080$, respectively. On the other hand, the measured slope values for the small-scale roughness are $(\sigma/\tau)_b = 0.129$ and $0.084$, respectively; the former is 8% high and the latter is 5% high. If we compare to measured slope values from the raw height data, we have slope values of $(\sigma/\tau)_r = 0.095$ and $0.041$, respectively, which are 12% and 49% too low as compared to the best-fit values. The raw data values reflect the influence of the gentler slopes of the large-scale roughness components. The closer agreement of the best-fit $(\sigma/\tau)_b$ and mechanically-measured small-scale roughness $(\sigma/\tau)_m$ slopes illustrates the importance of doing a roughness length-scale separation when trying to use mechanical roughness measurements as input to a model.

We also present a sensitivity study for the bead-blasted steel surfaces in Figures 7 and 8. The same measured BRDF data from Figures 4 and 5 are shown, but the curves are calculated from the reflection model using slope values $(\sigma/\tau)_m$ that bound the variability in the *measured* small-scale roughness slopes $(\sigma/\tau)_m$. In Figure 4, the model results fall below the measurements, whereas in Figure 5, the upper/lower model results tend to bracket the measurements.

The He-Torrance wave-optics model thus appears to work very well for the bead-blasted steel surfaces; this follows because the height distributions and autocorrelation functions are close to Gaussian. Moreover, the separation of roughness length scales appears to be very useful.

### 5.2. Ground glass with aluminum coating

For the two ground glass surfaces, GGAL120 (roughest) and GGAL240 (smoothest), the histograms and the autocorrelation functions (ACF) for the high frequency small-scale component of the roughness are shown in Figure 9. The fitted Gaussian curves agree moderately well suggesting that the high-frequency small-scale roughness components are nearly Gaussian. However, the grinding process itself implies that the roughness should not be Gaussian. To explain this, the height histogram and ACF for the *raw height data* of surface GGAL120 are shown in Figure 10. The associated histogram is nearly Gaussian but slightly skewed to the right toward higher heights, consistent with a grinding process that removes more peaks than valleys. On the other hand, the associated autocorrelation function is rather more exponentially distributed than Gaussian. This is consistent with the "jagged" appearance observed under a microscope. The statistical data imply that the ground glass surfaces contain a high-frequency, small-scale Gaussian roughness component (statistics in Figure 9) superposed on a low-frequency large-scale "jagged" roughness component. The small-scale, high-slope roughness is expected to dominate the light scattering.

The last statement is consistent with the following observation: For the two ground glass surfaces, the measured BRDF distributions turn out to be surprisingly similar,[35] differing by only a few percent. The similarity suggests that the small-scale, high-slope structures of the two surfaces are quite similar. That is confirmed by the data fitting, since nearly equal best-fit slopes are inferred. The large-scale roughness of the two surfaces, though quite different (i.e., $\sigma_r = 2.66\mu$m vs. $1.63\mu$m, Table 1), has little influence on the angular distribution of the scattered light. On the other hand, the small-scale roughness heights are less different ($\sigma_m = 0.86\mu$m vs. $0.61\mu$m, Table 1) as are the measured small-scale roughness slopes ($(\sigma/\tau)_m = 0.154$ vs. $0.130$, Table 1). The best-fit results for the slopes of the two surfaces from the wave-optics BRDF model (i.e., $(\sigma/\tau)_b = 0.166$ vs. $0.158$, Table 1) differ by about 5%, and are reasonably close to those for the small-scale roughness slopes. Inasmuch as the measured BRDF distributions for the two surfaces are virtually identical, we display results only for one surface, the roughest aluminized ground glass surface, GGAL120.

Incidence-plane BRDF measurements and data fitting results for the roughest ground glass surface are shown in Figure 11. A similar comparison over the reflection hemisphere is shown in Figure 12. A sensitivity study using the variation in the *measured* small-scale roughness slope $(\sigma/\tau)_m$ is shown in Figure 13.

The BRDFs in Figures 11 to 13 show Gaussian-like curves only for $10^\circ$ incidence. An off-specular peak is apparent for larger angles of incidence. The fittings of the He-Torrance model are generally good except that the model overestimates the magnitude of the off-specular peaks at incidence angles of $60^\circ$ and higher. The errors are most likely due to the shadowing/masking term in the model. A better shadowing/masking factor could reduce those errors. The "jagged" large-scale roughness only makes the effects more apparent. The best-fit slope value is about 8% higher than the measured value. For completeness, the effects of surface non-uniformity may be inferred from Figure 13, where it is clear that the measured slopes $(\sigma/\tau)_m$ yield BRDF predictions that fall somewhat above the best-fit predictions.

The He-Torrance model has a relatively good performance for the ground-glass surfaces. Although the fitting results are not as satisfactory as those for the bead-blasted surfaces, the model predicts the off-specular peaks with moderate magnitude errors.

### 5.3. Acid-etched glass with aluminum coating

The aluminized acid-etched glass is much smoother than the other test surfaces (Table 1). On the other hand, the surface is sufficiently rough so that no visible mirror reflection can be observed except at high grazing angles of incidence. The small-scale roughness is very close to Gaussian, as shown in Figure 14. Therefore, good comparisons with the He-Torrance model are expected.

Incidence-plane BRDF measurements and data fitting are shown in Figure 15. Note the log ordinate; there is virtually no diffusely scattered light. Also, no off-specular peak is observed due to the gentle slope of the surface-heights. The fittings of the data to the He-Torrance model are very good, except that the model slightly underestimates the maximum reflectance in the specular direction for large angles of incidence (more than $60^\circ$). The slope value obtained from the data fitting is $(\sigma/\tau)_b = 0.023$, essentially the same as the measured value of $(\sigma/\tau)_m = 0.024$ (for the small-scale roughness component). By doing a sensitivity study (not shown), and varying the mechanically-measured slope ($(\sigma/\tau)_m = 0.024$) by the observed surface non-uniformity (of -/+ 5.3%), the corresponding upper and lower bounds essentially bracket the measured data in Figure 15. The emergence of peaks is very sensitive to the slope values.

The He-Torrance model works well for this acid-etched glass surface. The positions and the lateral shapes of the reflection lobes are accurate. The underestimation of the maximum BRDF values is acceptable for our applications due to the limited dynamic ranges of human vision and display devices. Our surface characterization method is less necessary in this case. Although the measured slope is close to the best-fit result, the improvement is not significant. The height statistics suggest that this surface has only a single scale of roughness.

## 6. CONCLUSION

In this work, we experimentally study the relation between the surface-height statistics and the angular distribution of first-surface light scattering from several rough metal surfaces. The surface-heights were measured with a surface profilometer; the BRDFs of the surfaces were measured with a gonioreflectometer.

An analytical model based on the Kirchhoff approximation, the He-Torrance model,[2] was fit to the measured BRDFs of the rough metal surfaces. The fittings show that the model is able to describe the first-surface scattering of rough metallic surfaces that have multiple scales of roughness and near-Gaussian surface-height distributions, with an accuracy appropriate for computer graphics applications. The good agreement between the model and measurements implies that only one scale of roughness dominates the light scattering behavior.

The light scattering distributions are primarily attributable to the surface-roughness components with the steepest slopes.[31] We propose a composite roughness model, and with a filter, we extract the steepest-slope components from the surface profilometer measurements. Using the statistics of that component (i.e., the roughness slope $(\sigma/\tau)_m$) as input to the He-Torrance model, satisfactory agreement with the measured BRDFs was observed for our rough metal surfaces. The approach provides computer graphics practitioners with a practical method to obtain the input roughness data for use with a physical-optics-based light reflection model.


### Acknowledgements

The authors would like to thank Donald Greenberg, Steve Westin, and Hurf Sheldon of the Cornell Program of Computer Graphics for their encouragement and technical support. Equipment was donated by the Imaging Science Division of Eastman Kodak (Larry Iwan) and the Hewlett-Packard Company. This research was supported by the NSF Information Technology Research Program (ACI-0113851), the NSF Science and Technology Center for Computer Graphics and Scientific Visualization (ASC-8920219), the NSF Cornell Center for Materials Research (DMR-0079992) and the NSF Thermal Systems Program (CTS-9213183).


## REFERENCES


1. D. P. Greenberg, K. E. Torrance, P. S. Shirley, J. R. Arvo, J. A. Ferwerda, S. Pattanaik, E. P. F. Lafortune, B. Walter, S.-C. Foo, and B. Trumbore, "A framework for realistic image synthesis," in *Proceedings of SIGGRAPH 97, Comput. Graph. Proc., Annual Conference Series*, pp. 477–494, Aug. 1997.
2. X. D. He, K. E. Torrance, F. X. Sillion, and D. P. Greenberg, "A comprehensive physical model for light reflection," *Comput. Graph. (Proc. SIGGRAPH 91)* **25**, pp. 175–186, July 1991.
3. P. Beckmann and A. Spizzichino, *The scattering of electromagnetic waves from rough surfaces*, Pergamon Press, 1963.
4. A. Stogryn, "Electromagnetic scattering from rough, finitely conducting surfaces," *Radio Sci.* **2**(4), pp. 415–428, 1967.
5. F. E. Nicodemus, "Reflectance nomenclature and directional reflectance and emissivity," *Appl. Opt.* **9**(6), pp. 1474–1475, 1970.
6. B. T. Phong, "Illumination for computer generated pictures," *Communications of the ACM* **18**(6), pp. 311–317, 1975.
7. J. F. Blinn, "Models of light reflection for computer synthesized pictures," *Comput. Graph. (Proc. SIGGRAPH 77)* **11**, pp. 192–198, July 1977.
8. E. P. F. Lafortune, S.-C. Foo, K. E. Torrance, and D. P. Greenberg, "Non-linear approximation of reflectance functions," in *Proceedings of SIGGRAPH 97, Computer Graphics Proceedings, Annual Conference Series*, pp. 117–126, Aug. 1997.

9. R. L. Cook and K. E. Torrance, "A reflectance model for computer graphics," *ACM Trans. Graph.* **1**, pp. 7–24, Jan. 1982.
10. G. J. Ward, "Measuring and modeling anisotropic reflection," *Comput. Graph. (Proc. SIGGRAPH 92)* **26**, pp. 265–272, July 1992.
11. B. G. Smith, "Geometrical shadowing of a random rough surface," *IEEE Trans. Ant. Prop.* **15**, pp. 668–671, Sept. 1967.
12. E. I. Thorsos, "The validity of the Kirchhoff approximation for rough surface scattering using a gaussian roughness spectrum," *J. Acoust. Soc. Am.* **83**, pp. 78–92, Jan. 1988.
13. S. Marschner, S. Westin, E. Lafortune, and K. Torrance, "Image-based measurement of the bidirectional reflectance distribution function," *Applied Optics* **39**, pp. 2592–2600, June 2000.
14. K. J. Dana, "BRDF/BTF measurement device," in *Proceedings of the International Conference on Computer Vision*, pp. 460–466, IEEE Computer Society, IEEE Computer Society Press, (Los Alamitos, Calif.), 2001.
15. W. Matusik, H. P. Pfister, M. Brand, and L. McMillan, "A data-driven reflectance model," *ACM Transactions on Graphics* **22**, pp. 759–769, July 2003.
16. K. E. Torrance and E. M. Sparrow, "Theory for off-specular reflection from roughened surfaces," *J. Opt. Soc. Am.* **57**, pp. 1105–1114, 1967.
17. K. A. O'Donnell and E. Mendez, "Experimental study of scattering from characterized random surfaces," *J. Opt. Soc. Am. A* **4**, pp. 1194–1205, July 1987.
18. P. F. Gray, "A method of forming optical diffusers of simple known statistical properties," *Opt. Acta* **25**, pp. 765–775, Aug. 1978.
19. M.-J. Kim, J. C. Dainty, A. T. Friberg, and A. J. Sant, "Experimental study of enhanced backscattering from one- and two-dimensional random rough surfaces," *J. Opt. Soc. Am. A.* **7**, pp. 569–577, Apr. 1990.
20. M. E. Knotts and K. A. O'Donnell, "Measurement of light scattering by a series of conducting surfaces with one-dimensional roughness," *J. Opt. Soc. Am. A.* **11**, pp. 697–710, Feb. 1994.
21. J. Q. Lu, J. A. Sánchez-Gil, E. R. Méndez, Z.-H. Gu, and A. A. Maradudin, "Scattering of light from a rough dielectric film on a reflecting substrate: diffuse fringes," *J. Opt. Soc. Am. A* **15**, pp. 185–195, Jan. 1998.
22. E. I. Chaikina, A. G. Navarrete, E. R. Méndez, A. Martínez, and A. A. Maradudin, "Coherent scattering by one-dimensional randomly rough metallic surfaces," *Appl. Opt.* **37**, pp. 1110–1121, 1998.
23. H. E. Bennett, "Specular reflectance of aluminized ground glass and the height distribution of surface irregulatities," *J. Opt. Soc. Am.* **53**, pp. 1389–1394, 1963.
24. D. H. Hensler, "Light scattering from fused polycrystalline aluminum oxide surfaces," *Appl. Opt.* **11**, pp. 2522–2528, Nov. 1972.
25. E. Marx and T. V. Vorburger, "Direct and inverse problems for light scattered by rough surfaces," *Appl. Opt.* **29**, pp. 3613–3626, Sept. 1990.
26. L. X. Cao, T. V. Vorburger, A. G. Lieberman, and T. R. Lettieri, "Light-scattering measurement of the rms slopes of rough surfaces," *Appl. Opt.* **30**, pp. 3221–3227, Aug. 1991.
27. M. E. McKnight, T. V. Vorburger, E. Marx, M. E. Nadal, P. Y. Barnes, , and M. A. Galler, "Measurements and predictions of light scattering by clear coatings," *Appl. Opt.* **40**, pp. 2159–2168, May 2001.
28. G. R. Valenzuela, "Scattering of electromagnetic waves from a tilted slightly rough surface," *Radio Sci* **3**, pp. 1057–1066, 1968.
29. G. S. Brown, "Backscattering from a gaussian-distributed perfectly conducting rough surface," *IEEE Trans. Ant. Prop.* **26**, pp. 472–482, May 1978.
30. S. T. McDaniel and A. D. Gorman, "An examination of the composite-roughness scattering model," *J. Acoust. Soc. Am.* **73**, pp. 1476–1486, May 1983.
31. Y. Yang and R. O. Buckius, "Surface length scale contributions to the directional and hemispherical emissivity and reflectivity," *Journal of Thermophysics and Heat Transfer* **9**(4), pp. 653–659, 1995.
32. H. Li and K. E. Torrance, "Background data for validation of the He-Torrance model," *Tech. Rep. PCG-05-02*, Program of Computer Graphics, Cornell University, Ithaca, NY, 2005.
33. S. C. Foo, "A gonioreflectometer for measuring the bidirectional reflectance of material for use in illumination computation," *Master's thesis*, Cornell University, Ithaca, NY, 1996.

34. H. Li, S. C. Foo, K. E. Torrance, and S. H. Westin, "Automated three-axis gonioreflectometer for computer graphics applications," in *Advanced Characterization Techniques for Optics, Semiconductors, and Nanotechnologies II, Proc. SPIE* **5878**, SPIE, Aug. 2005.
35. H. Li and K. E. Torrance, "Validation of the gonioreflectometer," *Tech. Rep. PCG-03-2*, Program of Computer Graphics, Cornell University, Ithaca, NY, 2003.
36. P. Shirley and K. Chiu, "Notes on adaptive quadrature on the hemisphere," *Tech. Rep. 441*, Department of Computer Science, Indiana University, Bloomington, IN, 1994.
37. E. D. Palik, ed., *Handbook of optical constants of solids*, Academic Press, London, UK, 1997.

## Appendix A: He-Torrance BRDF model

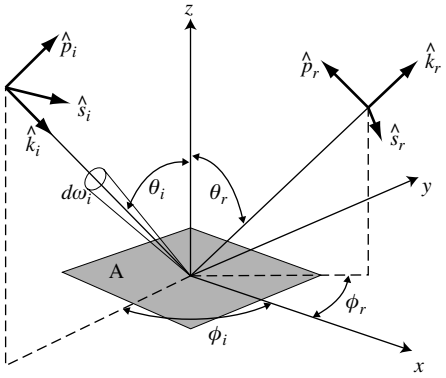


**Figure A1:** Coordinate system

The He-Torrance BRDF model is based on the vector form of the Kirchhoff approximation, applies for arbitrarily-polarized incident light, and describes specular, directionally diffuse, and uniformly diffuse scattering with three terms.[2] The angular distribution of scattered light depends on wavelength, incident and reflection angles, two roughness parameters, and the index of refraction. The coordinate system is shown in Figure A1, where $A$ is the area of the mean plane of the surface; $\hat{k}$ is the unit vector in the wave direction; and $\hat{s}$ and $\hat{p}$ are the $s$ and $p$ polarization unit vectors. In computer graphics we are most interested in the BRDF for unpolarized incident light. For that case, the BRDF equations greatly simplify and are presented here.

Assumptions of the model:

- Local radius of curvature of the surface is large compared to the illuminating wavelength;
- The surface-height and autocorrelation function are Gaussian distributed;
- A single roughness length scale;
- Plane, uniform, and isotropic surfaces.

The BRDF will be denoted here by the symbol $\rho_{bd}$. Equations for the BRDF:

$$\rho_{bd} = \rho_{bd}\left(\lambda, \sigma_0, \tau, \bar{n}(\lambda), a(\lambda)\right) = \rho_{bd,sp} + \rho_{bd,dd} + \rho_{bd,ud} \tag{5}$$

The specular reflection term:

$$\rho_{bd,sp} = \frac{\rho_s}{\cos\theta_i d\omega_i} \cdot \Delta; \tag{6}$$

$$\rho_s = |F|^2 \cdot e^{-g} \cdot S \tag{7}$$

$$\Delta = \begin{cases} 1 & \text{if in specular cone} \\ 0 & \text{otherwise} \end{cases} \tag{8}$$

$$|F^2| = \frac{1}{2}(F_s^2 + F_p^2) = f(\theta_i, \theta_r, \bar{n}(\lambda)) \tag{9}$$

$$g = \left[\frac{2\pi\sigma}{\lambda}\left(\cos\theta_i + \cos\theta_r\right)\right]^2 \tag{10}$$

$$\sigma = \sigma_0 \cdot \left[1 + \left(\frac{z_0}{\sigma_0}\right)^2\right]^{-1/2} \tag{11}$$

$$\sqrt{\frac{\pi}{2}} z_0 = \frac{\sigma_0}{4}\left(K_i + K_r\right) \cdot \exp\left(-\frac{z_0^2}{2\sigma_0^2}\right) \tag{12}$$

where $\rho_s$ is the specular reflectivity, $|F^2|$ is the Fresnel reflectivity for unpolarized light evaluated at the bisecting angle given by $\cos^{-1}\left(\left|\hat{k}_r - \hat{k}_i\right|/2\right)$, $\Delta$ is a delta function, $\bar{n}$ is the index of refraction, $\sigma$ is the apparent RMS roughness, $\sigma_0$ is the RMS roughness, and $\tau$ is the autocorrelation length.

The directional diffuse term:

$$\rho_{bd,dd} = \frac{|F^2|}{\pi} \cdot \frac{G \cdot S \cdot D}{\cos\theta_i \cos\theta_r}; \tag{13}$$

$$G = \left(\frac{\lambda}{2\pi}\frac{\vec{v}\cdot\vec{v}}{v_z}\right)^2 \cdot \frac{1}{\left|\hat{k}_r \times \hat{k}_i\right|^4} \cdot \left[(\hat{s}_r \cdot \hat{k}_i)^2 + (\hat{p}_r \cdot \hat{k}_i)^2\right] \cdot \left[(\hat{s}_i \cdot \hat{k}_r)^2 + (\hat{p}_i \cdot \hat{k}_r)^2\right] \tag{14}$$

$$S = S(\theta_i) \cdot S(\theta_r) \tag{15}$$

$$S(\theta_i) = \left(1 - \frac{1}{2}\text{erfc}(\frac{\tau\cot\theta_i}{2\sigma_0})\right)/(\Lambda(\cot\theta_i)+1) \tag{16}$$

$$S(\theta_r) = \left(1 - \frac{1}{2}\text{erfc}(\frac{\tau\cot\theta_r}{2\sigma_0})\right)/(\Lambda(\cot\theta_r)+1) \tag{17}$$

$$\Lambda(\cot\theta) = \frac{1}{2}\left\{\frac{2}{\pi^{1/2}} \cdot \frac{\sigma_0}{\tau\cot\theta} \cdot \exp\left[-\left(\frac{\tau\cot\theta}{2\sigma_0}\right)^2\right] - \text{erfc}\left(\frac{\tau\cot\theta}{2\sigma_0}\right)\right\} \tag{18}$$

$$D = \frac{\pi^2\tau^2}{4\lambda^2} \cdot \sum_{m=1}^{\infty} \frac{g^m e^{-g}}{m! \cdot m} \cdot \exp\left(-\frac{v_{xy}^2\tau^2}{4m}\right) \tag{19}$$

$$K_i = \tan\theta_i \cdot \text{erfc}\left(\frac{\tau}{2\sigma_0}\cot\theta_i\right), \quad K_r = \tan\theta_r \cdot \text{erfc}\left(\frac{\tau}{2\sigma_0}\cot\theta_r\right) \tag{20}$$

$$\vec{v} = \frac{2\pi}{\lambda}\left(\hat{k}_r - \hat{k}_i\right) = v_x\hat{x} + v_y\hat{y} + v_z\hat{z}, \quad v_{xy} = \sqrt{v_x^2 + v_y^2} \tag{21}$$

$$\hat{s}_i = \frac{\hat{k}_i \times \hat{n}}{|\hat{k}_i \times \hat{n}|}, \quad \hat{p}_i = \hat{s}_i \times \hat{k}_i \tag{22}$$

$$\hat{s}_r = \frac{\hat{k}_r \times \hat{n}}{|\hat{k}_r \times \hat{n}|}, \quad \hat{p}_r = \hat{s}_r \times \hat{k}_r \tag{23}$$

where $G$ is a geometrical factor, $S$ is the shadowing/masking factor,[11] and $D$ is a distribution function for the directional-diffuse reflection term.

The uniformly diffuse term:

$$\rho_{bd,ud} = a(\lambda); \tag{24}$$

where $a$ is constant (i.e. Lambertian), varying only with wavelength.

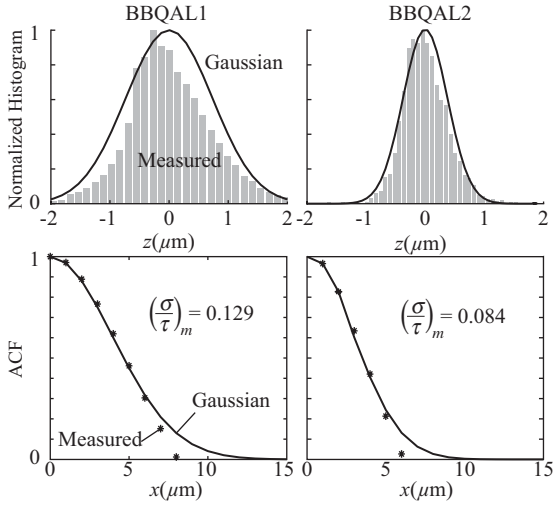


**Figure 3.** Small-scale roughness statistics for surfaces BBQAL1 and BBQAL2.

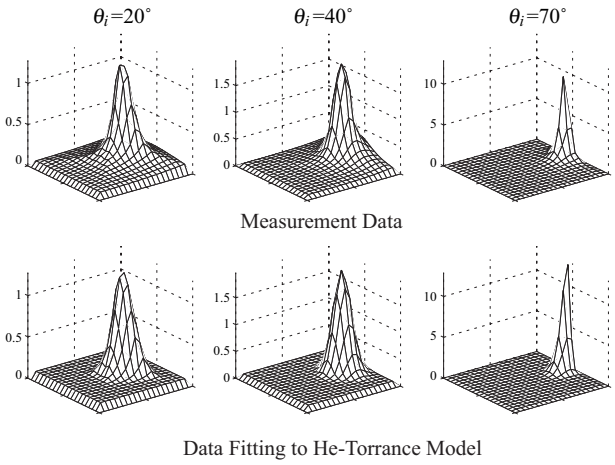


**Figure 6.** Comparison of measured BRDF (upper row) and best-fit model results (lower row) for surface BBQAL2 over the entire reflection hemisphere; $\lambda = 550$nm

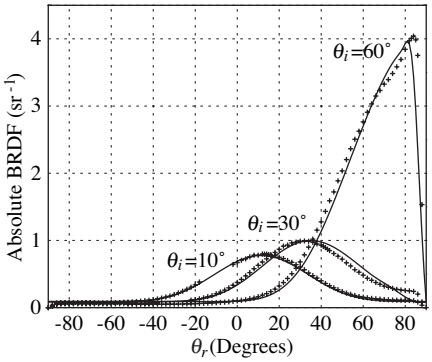


**Figure 4.** Incidence plane comparison of measured BRDF (symbols) and model results (curves) for surface BBQAL1, $\lambda = 550$nm. The measured slope was $(\sigma/\tau)_m = 0.129$; the best-fit BRDF model slope is $(\sigma/\tau)_b = 0.119$.

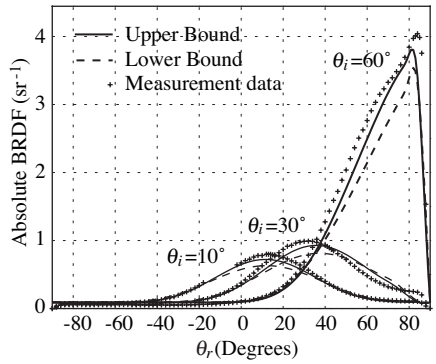


**Figure 7.** Incidence plane comparison of measured and predicted BRDFs for surface BBQAL1; $\lambda = 550$nm. The predicted BRDF used the mechanically-measured slopes $(\sigma/\tau)_m = 0.129$ -/+ $3.9\%$ as inputs.

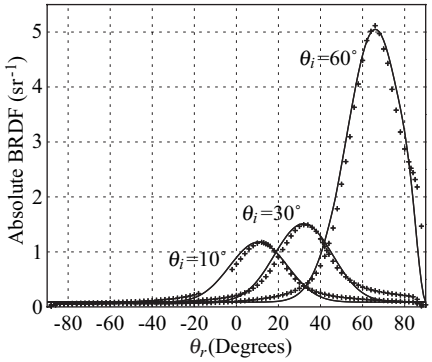


**Figure 5.** Incidence plane comparison of measured BRDF (symbols) and model results (curves) for surface BBQAL2, $\lambda = 550$nm. The measured slope was $(\sigma/\tau)_m = 0.084$; the best-fit BRDF model slope is $(\sigma/\tau)_b = 0.080$.

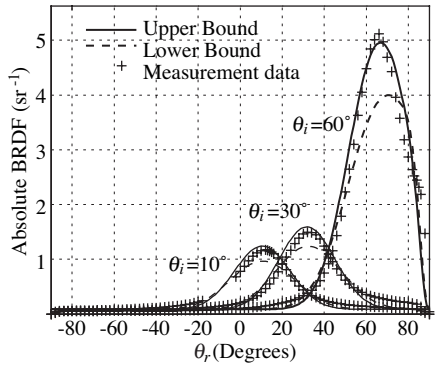


**Figure 8.** Incidence plane comparison of measured and predicted BRDFs for surface BBQAL2; $\lambda = 550$nm. In this figure, the predicted BRDFs used the mechanically-measured slopes $(\sigma/\tau)_m = 0.084$ -/+ $6.8\%$ as input.

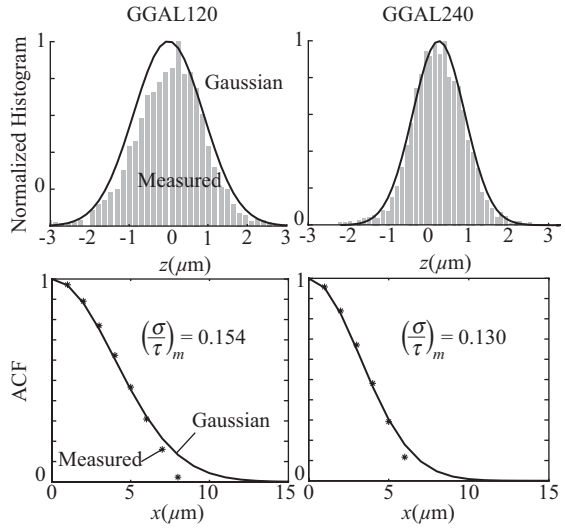


**Figure 9.** Small-scale roughness statistics for surfaces GGAL120 and GGAL240. The curves are Gaussian distributions.

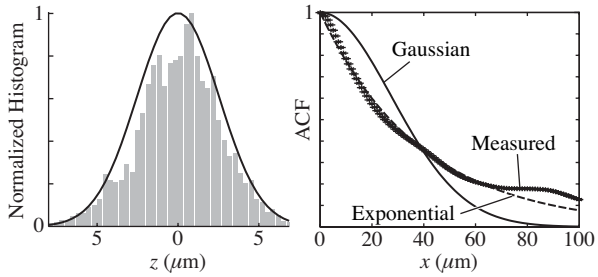


**Figure 10.** Aggregate roughness statistics for aluminized ground glass GGAL120 (measured slope $(\sigma/\tau)_m = 0.154$). The raw data were later separated into small-scale (Figure 9) and large-scale roughness components. The solid lines are Gaussian distributions; the dashed line is an exponential distribution.

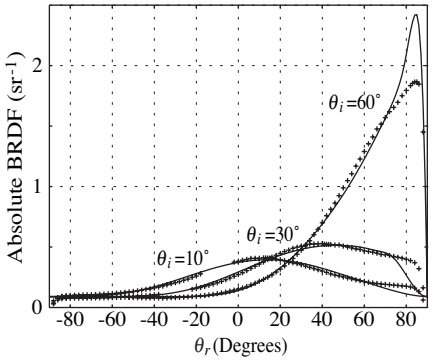


**Figure 11.** Incidence plane comparison of measured BRDFs (symbols) and best-fit model results (curves) for aluminized ground glass GGAL120 for several incidence angles $\theta_i; \lambda = 550$nm. The measured slope was $(\sigma/\tau)_m = 0.154$; the best-fit BRDF model slope is $(\sigma/\lambda)_b = 0.166$.

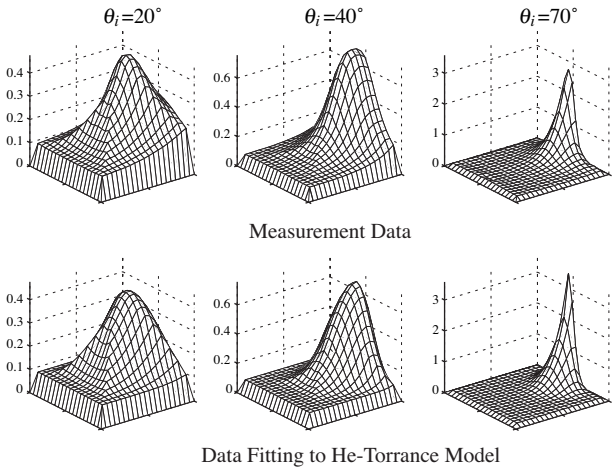


**Figure 12.** Comparison of measured BRDFs (upper row) and data fitting results (lower row) for surface GGAL120 ($(\sigma/\tau)_m = 0.154$), over the entire reflection hemisphere, for several incidence angles $\theta_i; \lambda = 550$nm. The best-fit model slope is $(\sigma/\lambda)_b = 0.166$.

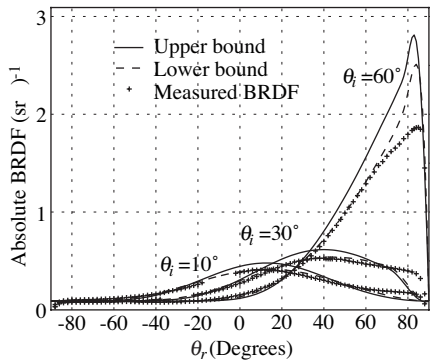


**Figure 13.** Incidence plane comparison of measured and predicted BRDFs for aluminized ground glass GGAL120 for three incidence angles $\theta_i; \lambda = 550$nm. In this figure, the predicted BRDFs used the mechanically-measured slopes $(\sigma/\tau)_m = 0.154$ -/+ 4.5% as inputs.

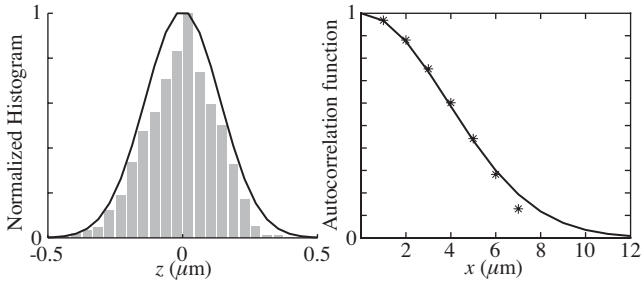


**Figure 14.** Small-scale roughness statistics for aluminized acid-etched glass NGGAL (measured slope $(\sigma/\tau)_m = 0.024$). The curves are Gaussian distributions.

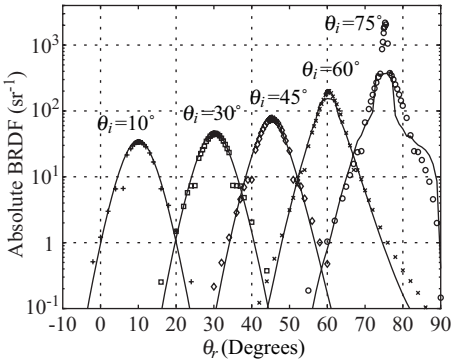


**Figure 15.** Incidence plane comparison of measured BRDFs (symbols) and best-fit model results (curves) for surface NGGAL for five incidence angles $\theta_i$; $\lambda = 550$nm. Note log scale. The measured slope was $(\sigma/\tau)_m = 0.024$; the best-fit BRDF model slope is $(\sigma/\tau)_b = 0.023$.